OXIDATION

MAJOR CHALLENGES IN THE DEVELOPMENT OF PHOTOCATALYTIC REACTOR FOR WATER PURIFICATION

Heterogeneous photocatalysis is one of the advanced oxidation technologies for air and water purification treatment and is documented in various references (1-4). It couples low energy ultraviolet (UV) light with semiconductors acting as photocatalysts, overcoming many of the drawbacks that exist for traditional water treatment methods. By using this technology *in-situ*, degradation of toxic compounds can be achieved both by oxidation (using photogenerated holes to oxidize organics, dyes, surfactants, and pesticides (5) and by reduction (using photogenerated electrons to reduce toxic metal ions (6).

The appeal of this process technology is the prospect of complete mineralization of pollutants to environmentally harmless compounds. Besides, the process use atmospheric oxygen as oxidants, the catalyst titanium dioxide (TiO_2) is cheap, stable, non-toxic, and can be used for extended periods without substantial loss of its activity. Moreover, it uses very low energy UV-A light (λ < 380 nanometers [nm]), resulting in energy requirement as low as 1 to 5 watts per square meters (W/m^2) of catalyst surface area, and more importantly, can even be activated even by sunlight (7).

In spite of the potential of this promising technology, development of a practical water treatment system has not yet been successfully achieved. There are several factors that impede the efficient design of photocatalytic reactors (8). Photocatalytic reactions are a complex, multi-phase reaction system. The solid photocatalyst is distributed within the continuous fluid phase, water and oxygen (or air), and the UV-light electronic phase. In these type of reactors, an additional engineering factor related to illumination of the catalyst becomes relevant. This is in addition to other conventional reactor complications such as reactant-catalyst contacting, flow patterns, mixing, mass transfer, reaction kinetics, catalyst installation, and temperature control. The illumination factor is of utmost importance since the amount of catalyst that can be activated determines the water treatment capacity of the reactor. The high degree of interaction between the transport processes, reaction kinetics, and light absorption leads to a strong coupling of the physico-chemical phenomena and it is one of the major hurdles in the technical development of a photocatalytic reactor.

The scale-up of fixed-bed photocatalytic reactors has been severely limited as reactor configurations have not been able to address the issue of mass transfer of pollutants to the catalyst surface. The new reactor design concepts must deal with this challenge. Earlier experimental studies by our group of catalyst-coated tube bundles (9), novel immersion type lamps (10), and rotating tube bundles revealed that the photocatalytic reaction is mainly diffusion (mass-transfer) controlled. The reaction occurs at the fluid-catalyst interface, and in most cases, the overall rate of reaction is limited to mass transport of the pollutant to the catalyst surface. In our earlier studies, we have enhanced mass transfer by increasing mixing of fluids through turbulence and introduction of baffles (11). In this work, a new photocatalytic reactor is considered that uses flow instability to increase reaction yield throughout the reactor volume.

Centrifugal Instability of Rotating Taylor-Couette Flow

The laminar flow confined within the annulus region between two co-axial cylinders with the inner one differentially rotating with respect to the outer suffers centrifugal instability, depending on the geometry and ro-

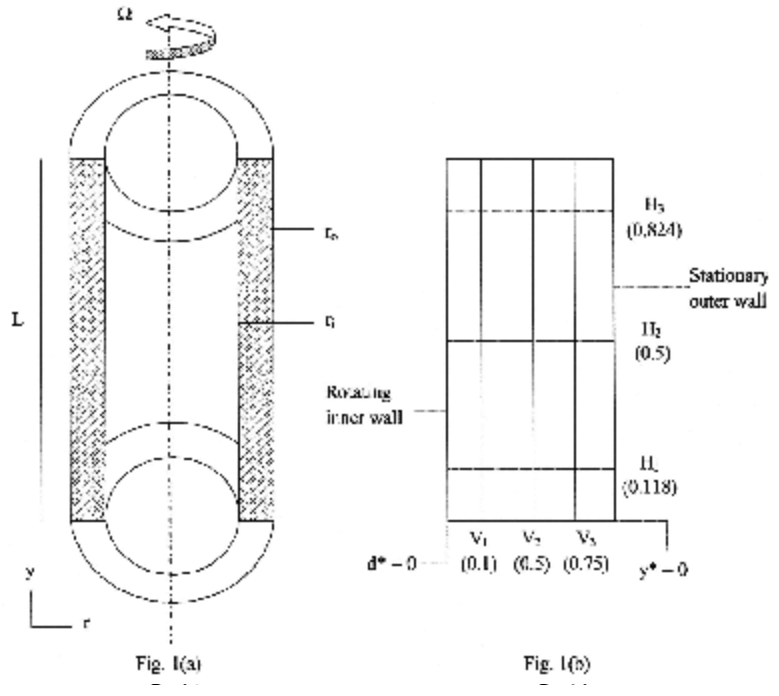

Figure 1. Schematic diagram of the Taylor vortex reactor (left), and location of the observation stations in the annular region to analyze flow behavior. D = 0 (rotating inner cylinder), d* = 1 (stationary outer wall), y* = 0 (bottom), y* = 1 (top).*

By Ajay K. Ray, Ph.D.
National University of Singapore

ISSN:0747-8291.

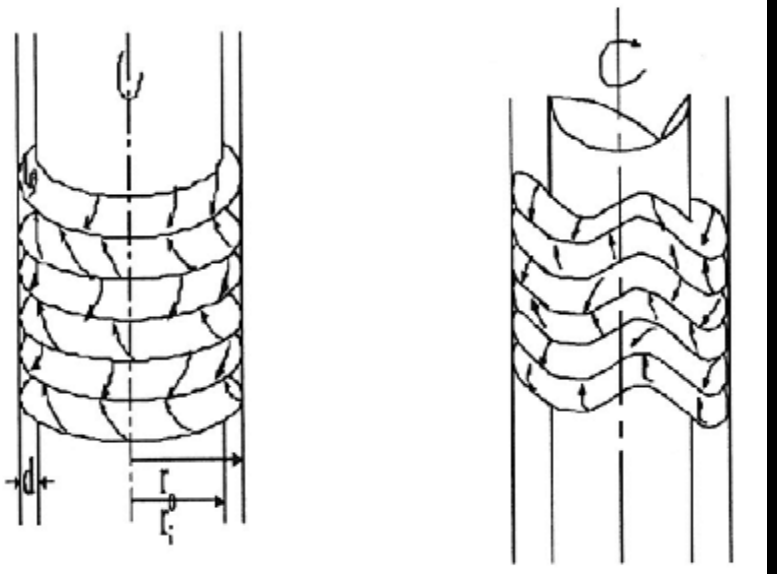

Figure 2. Vortices without and with circumferential waves.

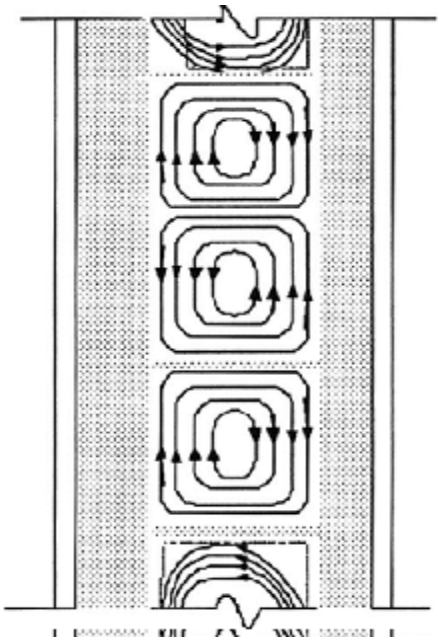

Figure 3. Schematic presentation of streamlines in vortical cells

tation rates. First experimental reporting was done by Taylor (12), although the first criteria of centrifugal instability was presented earlier by Rayleigh (13), who showed that an inviscid rotating flow to be unstable if the energy of rotation associated with fluid particle decreases radially outward.

Under such an unstable configuration, one notices the appearance of circumferential toroidal vortices in between the two cylinders and is known as Taylor-Couette vortices. These vortices evolve due to the adverse gradient of angular momentum that creates potential unstable arrangement of flow (14). Such an unstable condition arises naturally if the outer cylinder is held stationary while the inner cylinder is rotated at a sufficiently high rotation rate – an arrangement considered in the present study.

A schematic of the system is shown in Figure 1. The toroidal vortices that are formed in the annular region between the cylinders for a particular combination of the geometric arrangement and the inner cylinder rotation rates are shown in Figure 2. The non-wavy vortex flow is seen to appear as a consequence of primary instability as given by appropriate non-dimensional numbers like Taylor number and Reynolds (Re) number. When the Reynolds number is increased to somewhat higher values, then one sees the wavy vortex flow, also shown in Figure 3. (*Editor's note: This article has an Appendix that contains additional figures presented with the original paper. Due to space considerations, not all figures could be included with the printed version. The Appendix is available with the electronic version that is available at our web site: ultrapurewater.com.)*

In such an unstable condition, the annulus is filled with pair of counter rotating vortices. This can be viewed in Figures 3 and 4. Figure 4 also shows the boundary layer forming on the inner surface to have an axial periodicity. The boundary layer oscillates periodically between almost zero thickness to a maximain between the counter-rotating vortex pair, where the two shear layers approaching each other spews out a jet of fluid towards the outer wall. The fluid particles in their motion around the toroidal vortices come periodically in contact with the inner surface.

By assuming the annular gap, $d = (r_o - r_i)$, as small compared to the inner cylinder radius (r_i), where r_o is the outer cylinder radius, it has been shown by Taylor (12) that stability is dependent only on the ratio of the rotation rate of the outer cylinder to the rotation rate of the inner cylinder, (Ω_o/Ω_i), and a single parameter, called Taylor number, T_a, which can be defined as seen in Equation 1. (Editor's note: All equations for this article are together in a single Equations table.) From the stability theory for $0 \leq \Omega_o/\Omega_i \leq 1$ and large aspect ratio, it has been established that primary instability in the form of the appearance of Taylor vortices occurs at $T_{a,\,crit} \approx 1{,}708$.

A particle image velocitymetry (PIV) was used to measure the axial and radial velocities in a meridional plane for non-wavy and wavy Taylor-Couette flow in the annulus between a rotating inner cylinder and a fixed outer cylinder with fixed-end conditions by Wereley and Lueptow (15). It was shown that the vortices became stronger and the outflow between pairs of vortices was jet-like. Wavy vortex flow is characterized by azimuthal deformation of vortices both axially and radially.

According to their findings, it was also shown that significant transfer of fluid between neighboring vortices occurs in a cyclic fashion at certain points along an azimuthal wave so that while one vortex grows in size, the two adjacent vortices become smaller, and vice versa. Vortex cells were not independent as the significant transfer of fluid between adjacent vortices occurs in wavy flow regime. This aspect of the flow is important, because traditionally it is assumed that the vortex pair in Taylor-Couette vortices is independent of each other and is of the same size and it is customary to treat this as plug flow. But, the observation of Werely and Lueptow (15) is significant from the point of view of present application.

If indeed there is significant mass transfer between adjacent vortex pair, then that

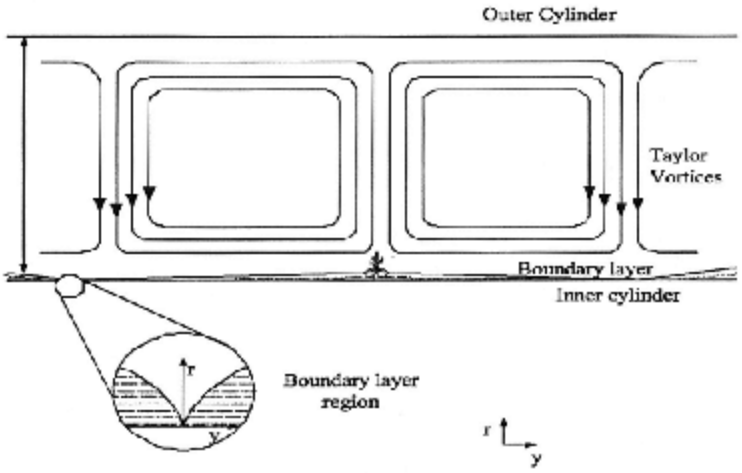

Figure 4. Radial mass transfer in Taylor-Couette flow.

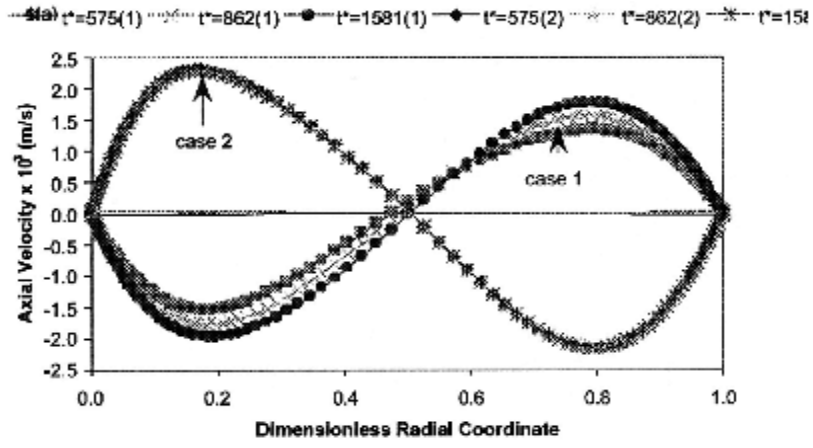

Figure 5. A comparison of the axial velocity.

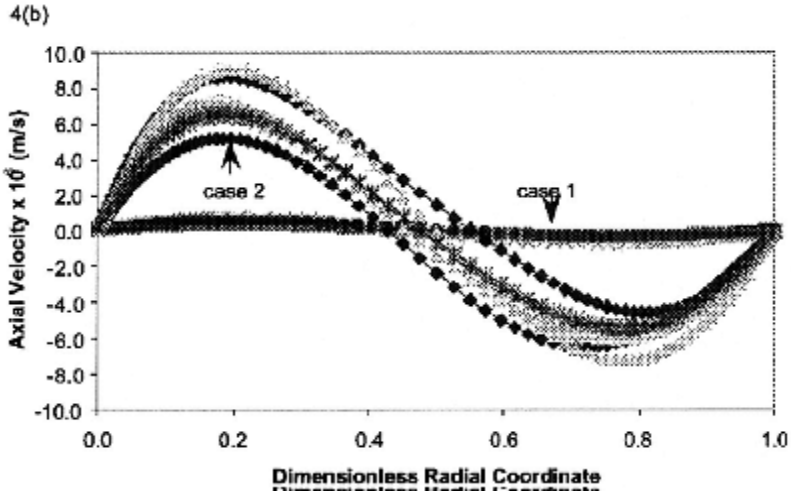

Figure 6. A comparison of the axial velocity.

can be used for additional benefit for the performance enhancement of the present reactor. The transfer of fluid particles between adjacent vortices occurs with a cyclic fashion as a particular vortex gains fluid from adjacent vortices. It has also been reported that the degree of transfer of fluid is greater at a Reynolds number equal to 253 than at either a higher or lower Reynolds number. In addition to flow into and out of adjacent vortices taking place periodically, the individual vortex centers also move both axially and radially in a cyclic fashion. Once again, the maximum departure in the radial direction is a strong function of the Reynolds number and is found to be a maximum for Re = 253.

In this work, we have considered a Taylor Vortex Photocatalytic (TVR) reactor, which is shown schematically in Figure 1, and a dimension of the reactor is given in Table A. In the present reactor, it is assumed that the outer surface of the inner cylinder is coated with TiO_2 photocatalyst and it is illuminated with a lamp placed inside the inner cylinder. Sczechowski, et al. (16) have reported their experimental studies related to enhancing the photo-efficiency of a TVR. But, they have used semiconductor photocatalyst particles as slurry in the fluid within the annulus. They have found that despite the photocatalyst being dispersed in the fluid, the useful reaction took place only periodically when the fluid was in contact with the illuminated inner cylinder surface. They reported three-fold increase in the photo-efficiency when the reactant was illuminated for less than 150 ms, and it stayed in dark for more than 1's.

The maximum photo-efficiency achieved by them was 30% at 300 revolutions per minute (rpm) of the inner cylinder when 10 grams per liter (g/L) loading of TiO_2 was used. The major problem of achieving higher photo-efficiency was related to the transport of purified fluid from the vicinity of the catalyst. Furthermore, their configuration suffers from the additional problem of separation of sub-micron size catalyst particles after the purification stage. Moreover, the working fluid is optically dense, and therefore, the light penetration depth is restricted to a distance that is of the order of the boundary layer thickness of the inner cylinder.

In view of all these factors we have considered, a TVR of similar geometry, but instead of a slurry type reactor, the photocatalyst was assumed to be immobilized (fixed) on the outer surface of the inner cylinder and a fluorescent lamp illuminates the inner cylinder on which the catalyst is immobilized, and in the presence of light the catalyst is activated and as a result the redox reaction takes place. Thus, one can use a very low level of catalyst loading, and simultaneously, eliminate the process of separation of catalyst particles after the purification stage. The enhanced purification has been obtained by using fluid dynamical instability associated with centrifugal instability in the cylindrical an-

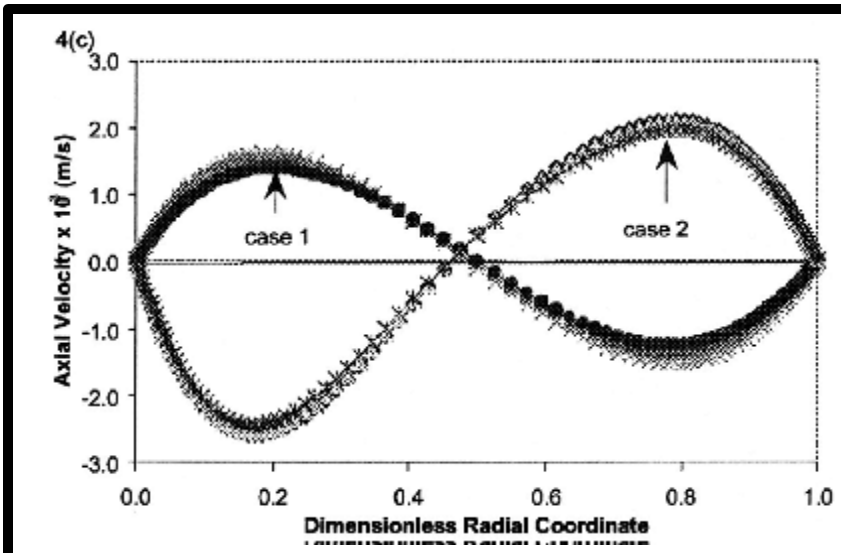

Figure 7. A comparison of the axial velocity.

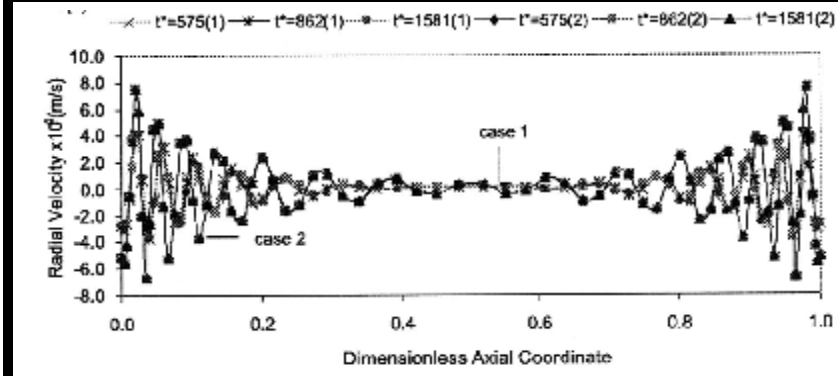

Figure 8. The axial velocity is plotted along the dimensionless axial direction.

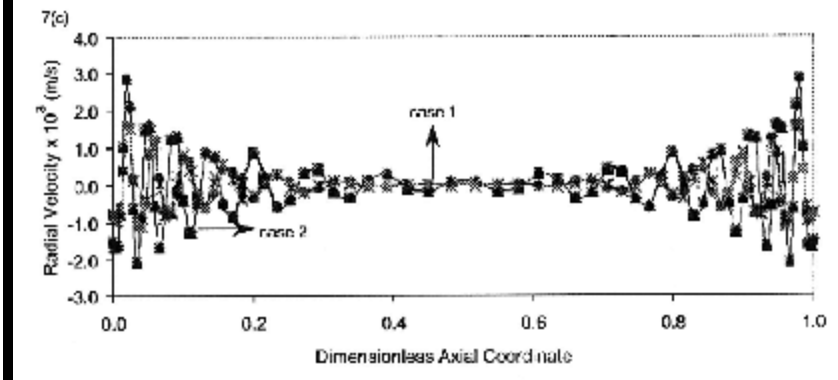

Figure 9. The axial velocity is plotted along the dimensionless axial direction.

nular geometry.

It is, therefore, essential to focus on the twin aspects, photocatalysis and centrifugal instability, in an annular cylindrical geometry. The residence time in the illuminated region is a function of the angular velocity of the re-circulating vortex as well as the size of the vortex. The latter, once again depends on the gap size and the number of vortices formed in a given length of the reactor. The two most important factors for unstable Taylor-Couette flow establishment are the aspect ratio (L/D) and the Reynolds number. The effect of aspect ratio on the flow development has been studied by Sengupta, et al. (17). In the present study we investigated the effect of Reynolds number on the formation of vortices and its effect on overall degradation of a pollutant.

Results and Discussion

Flow development. The performances of the reactor depends on the photo-efficiency of the photocatalytic process as well as on the mass transfer efficiency of the fluid from the vicinity of the rotating inner cylinder to the stationary outer cylinder and back within a single Taylor-Couette vortex. The latter depends on the primary instability of flow in setting-up of the vortical roles. This instability and associated mass transfer can be made more effective by initiating a secondary motion when additional mass transfer between neighboring roles through the wavy vortex flow would take place. This has been shown to be a strong function of Reynolds number by Werely and Lueptow (15) and it was reported that inter-role mass transfer is maximum for the chosen geometry in their experiment for Re = 253.

In the present set of computations, the same geometric parameters are chosen, including the aspect ratio, (AR = L/d) of the reactor. However, in the experiment, the starting protocol of the inner cylinder rotation was taken as quasi-static and the reported results were recorded after allowing the flow to develop further for 10 minutes after the attainment of the final rotation rate. In the present computations, the flow is started impulsively for the practical operation of the reactor in a shortest possible time period. For such an operation, the transient mass transfer depends strongly upon the vortices that are formed at initial times near the fixed end-caps of the reactor.

Since the rotating inner cylinder drives the flow inside the reactor and the rotation rates are low, it is quite adequate to consider the flow to be incompressible and solve the governing Navier-Stokes equation in primitive variable form as shown in Equations 2 and 3.

Furthermore, isothermal conditions can be assumed for both the flow evolution and chemical reaction calculations since the pollutant being oxidized into other products is present in trace amounts, and heat of reaction in photocatalytic reactions is usually negligible (18). The boundary conditions that are applied on the inner and outer cylindrical surface correspond to no-slip conditions. The end caps are considered to be a part of the outer cylinder and hence are stationary. The following boundary conditions are used for the numerical simulations. With reference to Figure 1, on the inner cylinder surface (Equations 4 and 5).

Equations 6 and 7 show that the simula-

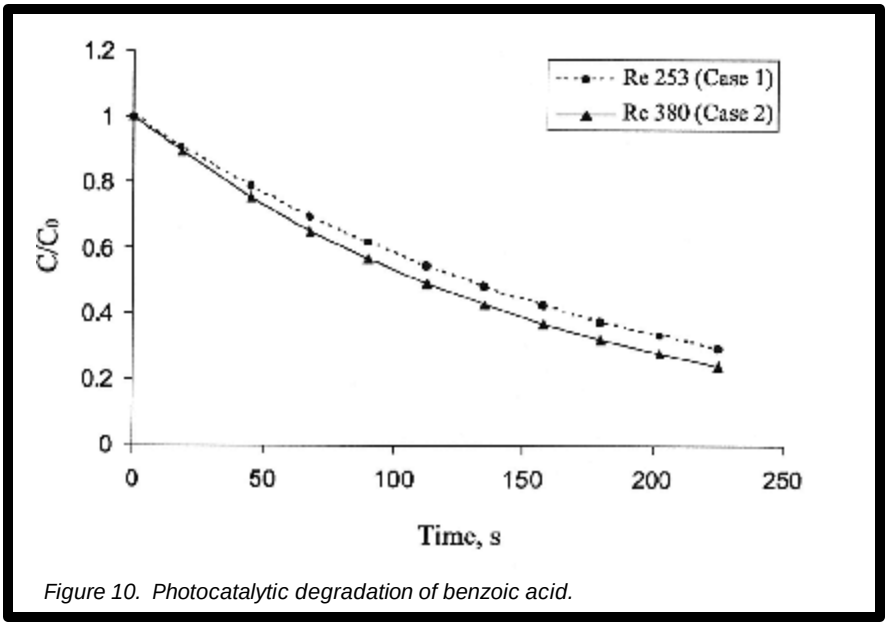

Figure 10. Photocatalytic degradation of benzoic acid.

tion is for the impulsive start of the rotation rate of the inner cylinder. The model pollutant considered in this work is benzoic acid with an initial concentration of 100 parts per million (ppm), while the initial mass fraction of oxygen (O_2) is taken to be equal to twice the stoichiometric requirement for the reaction given in Equation 8. The rate expression for photocatalytic degradation for benzoic acid used in this study is given by Equation 9 (19).

The amount of catalyst coating is assumed to be 3×10^{-3} kilograms per square meter (kg/m^2) (10). The density of the system is assumed to be constant and equal to that of water as the pollutant is present at very low concentration.

Computational details. In computing the flow, the three-dimensional Navier-Stokes equation is solved in primitive formulation by using the commercial software Fluent®. This is found adequate as the flow considered is laminar, and therefore, the need for resolving large ranges of wave numbers and circular frequencies is not necessary. In solving the governing equations, no simplification is made regarding symmetry and reflection of the solution. The time-accurate solution was obtained instead of assuming an *a priori* steady state. The geometric dimensions chosen for the reactor are identical to the value reported in Werely and Lueptow (15).

The reactor is considered to be operating in a batch mode, purifying 1.136 liters (L) of water at a time. The three different rotation speeds of the inner cylinder is considered 0.655, 0.984, and 1.638 rad/s, which result in Reynolds numbers of 253, 380, and 633, respectively. The rotation speed is varied to obtain the Reynolds number of 1.5 and 2.5 times, respectively, that in the first case the Re = 253. The present reactor provides 0.116 m^2 of illuminated catalyst surface area and an illuminated catalyst density of 102 square meters per cubic meters (m^2/m^3).

For generating grids within the annulus region of the geometry, every edge in three directions is defined with certain nodes. There are high-shear regions near the inner cylinder wall, the outer cylinder wall, and the end-cap regions. Therefore, axial and radial derivatives of all physical variables across such layers would be larger than in the azimuthal direction, and consequently, more grid points are taken in axial and radial directions compared to the azimuthal direction. In order to incorporate these, grid points are taken more clustered in two ends and next to inner and outer wall.

To enhance the direct mapping of grid from upper wall to bottom wall, the total geometry is separated into two volumes by a brick. Two interior planes are created by this process within the annular space that was used to analyze our results at the time of post processing. Grid points along the three directions are taken as follows: $r \times \theta \times h = 100 \times 40 \times 75$. Fluent pre-processor GAMBIT© 1.1 is used to create geometry and generate grid for both cases. There are 0.3 million cells, 907,000 total quadrilateral faces (3,000 inner wall faces, 11,000 outer wall spaces, 15,000 interior plane faces, and 878,000 rest of interior plane faces). The total numbers of nodes are 307,040. The present set of computation of Navier-Stokes equation for Taylor-Couette geometry is expensive. The one without reaction was computed in a 1.5-Gb RAM Windows NT workstation and it took 78 hours of actual time for simulation results of 10 s.

Equations 2 and 3 are solved subject to the boundary conditions and initial conditions defined in Equations 4 through 7 within the annulus between the cylinders as shown in Figure 1. The results are shown in the radial-axial (r-y) plane and along the three sets of horizontal (H_1-H_3) and vertical lines (V_1-V_3), as indicated in Figure 1.

A brief description of the method is given in the next section. The solver is based on solving Equations 2 and 3 in a sequential manner by a control volume based technique, using the following three steps. First, the computing domain was separated into discrete control volume, using a computational grid. The governing equations were time advanced in integral form for each computational cell to yield algebraic equations for the discrete dependent variables, such as velocity components, pressure, and conserved scalars. Finally, the discrete equations were linearized into a set of algebraic equations, which were solved to yield updated variables.

For the separation process, the familiar QUICK scheme was used for the momentum and species equations, as this is a higher-order accurate scheme with minimum numerical dissipation that is implicit with the separation. The solver uses finite volume method in solving the Navier-Stokes equation.

Simulation results. The following non-dimension is used in order to be able to compare results to reported results in literature. The annulus gap, d, is used as length scale while the speed ($W r_i$) imposed on the inner cylinder surface is used as the velocity scale. Thus, the dimensionless time scale used is $t^* [\equiv t(\Omega r_i)/d]$. Since the water pollutant pollutant is present in a trace quantity, it is expected that the chemical reaction will not influence the fluid dynamic behavior of the system. To show this two sets of computations were initiated from t = 0, one with the chemical reaction, while in the other only the fluid flow was computed and the results compared. It was observed that flow field was identical.

The numbers of vortices formed in the three configurations (see Table A and Figure A of the Appendix) are 5.75, 6.5, and 5.0 for Configuration 1, Configuration 2, and Configuration 3, respectively. It can be clearly seen that the number of vortices formed are maximized when the Reynolds number is 1.5 times the reference case (Re = 253). Moreover, when the

Reynolds number is 2.5 times that of the reference case, we see that the flow has not been completely established in the entire region. The vortex at the top is degenerated and the vortices in the middle section are also not as compact when compared to the other cases.

We observed the following for Configuration 2 compared to configuration 1 (reference case): 1. It reaches steady state faster; 2. The number of vortices per unit length is more; 3. The vortices move faster towards center from end; and 4. The intensity (i.e., magnitude) of both axial and radial component of velocity is more than the reference case (i.e., Re = 253). It can be observed that for the simulated case with impulsive start, that the optimum Re = 380 instead of 253, as was found by Werely and Lueptow (15). The deviation from the experimental results probably is due to the impulsive start of the simulated reactor as opposed to the quasi-static start in the experimental case. Since the Configuration 2 gives better results than the Configuration 3, for all subsequent reported results comparison are made between the Configuration 1 and Configuration 2.

In Figures 5 through 7, the axial velocity as a function of dimensionless radial coordinate is plotted for various time instants at the observation stations H_1, H_2, and H_3. Comparing the velocity profile of Configurations 1 and 2, the velocity magnitudes are 1.3 times higher for Configuration 2 than that for the reference case. The results from Figure 5 also indicate that for Configuration 2 the rate of change of axial velocity is almost negligible and therefore, the flow reaches steady state faster than that of the reference case. From Figure 6, the axial velocities demonstrate that Taylor-Couette vortices move faster toward the middle part when the Reynolds number is higher. In general for both cases, since the middle section is at the center (y* = 0.5), there the axial velocity is smallest in magnitude (about 4 order of magnitude lower) when compared to the other two observation stations.

The radial component of velocity is plotted (see Figure B in the Appendix) in the annular gap at the three different heights at three different non-dimensional times. In Configuration 2, an inflow of fluid moves towards the inner cylinder for all the indicated times, while for Configuration 1 up to t* = 862 the fluid moves towards the inner cylinder, but at t* = 1581 the fluid moves toward the outer cylinder. The rate of change of radial velocity is much slower for Configuration 2 than for Configuration 1, indicating the flow will reach steady state faster when Re = 380.

The magnitude of the radial velocities is the smallest for both configurations (Figure B in the Appendix). The research also indicated that the flow does not show the formation of Taylor-Couette vortices in the middle part of the reactor for the reference case, but for Configuration 2 the vortices have started forming in the center. Thus, higher Re is responsible for formation of vortices at the middle part of the reactor.

The axial velocity (seen in Appendix Figure C) is plotted along the dimensionless axial direction at observation stations V_1, V_2 and V_3. For both the configuration at smaller times, the Taylor-Couette vortices are formed at the ends and as time progresses more and more of these are formed covering the middle part. The magnitude of both axial and radial velocities is on an average 1.5 times larger for Configuration 2 than for the reference case.

From Figures 8 and 9 (and Figures C and D in the Appendix), it is evident that for at higher Reynolds numbers the vortices move faster to the middle part. This is of great importance as the faster movement and formation of vortices in the entire reactor is the basis for improvement of performance of the photocatalytic Taylor vortex reactor. Of specific interest is the plot of the axial velocities in the middle of the annulus at V_2. If indeed the vortices formed were like a plug flow, then this velocity component along this line would have been zero.

The very fact that the velocity component alternates in sign is indicative of the fact that the vortex centers not only execute axial waviness, but also show significant radial motion. Werely and Lueptow (15) also observed this experimentally where they showed such motions for all Reynolds numbers between 131 to 1,221. They reported large excursions of axial motions for low Reynolds numbers while maximum radial motion of vortex centers were observed for Re = 253 as opposed to at Re = 380 in this present case. However, it has to be noted that in the present investigation the flow is started impulsively and not accelerated quasi-statically.

The velocity vector plots are shown for only the top half of the reactor (y* = 0.5 - 1.0) in a given *y- r* plane at t* = 879 when steady state has reached (Figure E in the Appendix). One can see weak vortices forming near the upper part of the left segment. There are regions along the height where one can see a jet-like flow starting from the inner wall moving towards the outer wall due to centrifugal action. In the segment between y* = 0.7 and 0.85, significant mixing of fluid is noticeable due to the formation of coherent vortices.

Once again, one can see the jet-like flow from inner to outer cylinder - although the trajectory of the fluid particles are not strictly straight. Moreover, there is no visible wall shear layer forming on the inner wall as has been shown in Figure 4. In the segment between 85% and the top of the reactor, the velocity vectors clearly shows recirculating rolls, although the axial lengths vary significantly due to end-wall effects. Also in this segment, apart from the jet-like regions, one can as well see small axial regions where a flow is established from the outer to the inner wall side. However, this cannot cover the entire radial gap because of centrifugal force acting on fluid particles near the inner wall.

For the same reasons one will not see a wall shear layer forming on the inner cylinder as has been shown in Figure 4. Instead, one would notice the formation of an internal layer after some time and associated full saddle point inside the flow domain. In retrospect, it appears that to resolve such internal layers, one should have finer grid in the interior, too. An internal band characterizes the formation of the internal layer where the flow is along the axis of the reactor (Figure F of the Appendix). This is seen to originate at the saddle points, one of which is marked in the figures with filled circle for different times.

The flow is seen to be axial in opposite direction across the saddle point. Such vertical lines are nothing but the internal layer. While at t* = 383, no such inner layers were seen, it is seen for the plot shown at t* = 575. Once this saddle point is seen to form, it does not seem to move as it can be traced at the same location at later times. It is also interesting to note that between t* = 671 and t* = 767, while the saddle point remains fixed, the velocity vectors indicate an increase in upward velocity above the saddle point while it decreases in downward direction. The velocity vectors inside the recirculating eddies show time dependent behavior, though it is not so pronounced near the middle section of the reactor where the eddies are either very weak or not formed. All of these unsteady events would lead to an increase of mass exchange between adjacent fluid cells.

Finally, in this section we want to discuss about the flow structure for the chosen parameters of this computation with an impulsive start of the reactor. This aspect is very important in the context of non-unique flow evolution due to different initial conditions referred to in Andereck, et al. (20). The flow structure that we have computed is significantly different than what has been experimentally visualized by Werely and Lueptow (15), although the geometric parameters and Reynolds number chosen are identical. This is due to the impulsive start of the present computed case as opposed to the quasi-static start in Werely and Lueptow (15) where the inner cylinder is accelerated from rest to its final value at the very slow rate of 0.3 Re per second.

Our research showed the flow structure for the two segments for t* = 1,054 (Figure G in Appendix). The time is not important as we have noted that the flow structure remains invariant beyond t* = 575. If one looks carefully one notices the jet-like flow structure between fluid cells. For example, one can notice an unidirectional jets emerging from the inner wall and approaching the outer wall. This is the expected jet structure indicated in the sketch of Figure 4. However, one can also notice the existence of bi-directional jets as marked by F and H.

A longer segment originating from the outer wall and moving towards the inner wall is met with a smaller segment where the flow is from the inner to outer wall. Then, we have marked a line J in the figure, which is the limiting case of the bi-directional jet when the width of the jet degenerates into a line and the merger line of the opposing jet becomes the saddle point. The notation U, B, and S in the figure indicate locations of unidirectional, bi-directional, and singular zones.

Photocatalytic reactions. To analyze the performance of the TVR, benzoic acid is considered as typical pollutant present in water with an initial concentration of 100 ppm. Pollutant degradation as integrated over the full reactor volume and is shown as function of time in Figure 10. It is to be noted that after 225s of operation, benzoic acid is degraded by about 69% and 76% respectively for Case 1 (Re = 253) and Case 2 (Re = 380). It clearly indicates the role of Taylor-Couette vortices in enhancing the rate of pollutant degradation.

At early times, the very rapid rate of degradation is due to the vortices that are form at the fixed ends where strong recirculating zones causes rapid mass transfer from inner to outer cylinder and back. Figure 10 illustrates that photocatalytic reaction is diffusion controlled, as the rate of degradation increases when Re is increased. Since in this case the vortices move faster towards center from the end caps and the magnitude of the vortices are also larger compared to when Re = 253.

A close scrutiny of Figures 5 through 9 (and Figures A through G) reveals that reaction is faster at either end where well-developed vortices are present, while the degradation rates are slower where Taylor-Couette vortices are not well formed (see also Appendix Figure H). The reaction takes place only in the shear layer of the inner cylinder where there are no Taylor-Couette vortices present.

Figure 10 clearly indicates the role of Taylor-Couette vortices in enhancing the rate of pollutant degradation. Moreover, the figures also indicate the possibility of operating the reactor in the transient mode by periodically switching the reactor on and off since during the transient phases the reaction proceed at a rapid rate due to the vortices near the end walls.

Table B compares the performance of a slurry reactor (19) with that of the two cases of Taylor vortex reactor (TVR) considered in this work for photocatalytic degradation of benzoic acid. The table clearly illustrates that increase in efficiency of TVR over the slurry reactor. One can observe 50.4% and 78.3% increase in efficiency for Taylor vortex reactor with Re = 253 and with Re = 380 respectively over a slurry reactor.■

References

1. Ollis, D. F.; Pelizzetti, E.; Serpone, N. (1989). in *Photocatalysis: Fundamentals and Applications*, Serpone, N.; Pelizzetti, E., eds., Wiley Interscience, New York, N.Y., p. 603 (1989).
2. Fox, M.A.; Dulay, M. T. "Heterogeneous Photocatalysis", *Chemical Review*, 93, p. 341 (1993).
3. Hoffmann, M.R.; Martin, S.T.; Choi, W.; Bahnemann, D.W. "Environmental Applications of Semiconductor Photocatalysis", *Chemical Review*, 95, p. 69 (1995).
4. Hermann, J. M. "Heterogeneous Photocatalysis: An Emerging Discipline Involving Multiphase Systems, *Catalytic Today*, 24, p. 157 (1999).
5. Halmann, M.M. "Photodegradation of Water Pollutants", CRC Press, New York, N.Y. (1995).
6. Chen, D. W.; Ray, A. K. "Removal of Toxic Metal Ions from Wastewater by Semiconductor Photocatalysis", *Chemical Engineering Science 56(4),* p. 1561 (2001).
7. Ray, A. K.; Beenackers, A. A. C. M. "Novel Swirl-Flow Reactor for Kinetic Studies of Semiconductor Photocatalysis", *AIChE Journal*, 43, p. 2571 (1997).
8. Mukherjee, P. S.; Ray, A. K. "Major Challenges in the Design of a Large-Scale Photocatalytic Reactor for Water Treatment", *Chemical Engineering Technology*, 22, p. 253 (1999).
9. Ray, A. K. "Design, Development and Experimentation of a New Photocatalytic Reactor for Water Treatment", *Chemical Engineering Science 54(16)*, p. 3113 (1999).
10. Ray, A. K.; Beenackers, A. A. C. M. "Novel Photocatalytic Reactor for Water Purification", *AIChE J.*, 44, 477 (1998).
11. Periyathamby, U.; Ray, A. K. "Computer Simulation of a Novel Photocatalytic Reactor Using Distributive Computing", *Chemical Engineering Technology 22 (10)*, p. 881 (1999).
12. Taylor, G. I. "Stability of a Viscous Liquid Contained between Two Rotating Cylinders", *Phil. Transcripts R. Soc.*, pp. A223, 289 (1923).
13. Rayleigh, L. "On the Dynamics of Revolving Fluids", scientific papers, Cambridge, England, 6, 447 (1920).
14. Chandrasekhar, S. "Hydrodynamics and Hydromagnetic Stability", pp. 273-340, Oxford University Press, Oxford, England (1961).
15. Werely, S. T.; Lueptow, R. M. "Spatio-Temporal Character of Non-Wavy and Wavy Taylor Couette Flow", *Journal of Fluid Mechanics*, pp. 364, 359 (1998).
16. Sczechowski, J.G.; Koval, C.A.; Noble, R. D. "A Taylor Vortex Reactor for Heterogeneous Photocatalysis", *Chemical Engineering Science 50(20),* p. 3163 (1995).
17. Sengupta, T. K.; Kabir, M. F.; Ray, A. K. "A Taylor Vortex Photocatalytic Reactor for Water Purification", *Industrial Engineering Chemical Research,* 40, p. 5268 (2001).
18. Chen, D. W.; Li, F.; Ray, A. K. "Effect of Mass Transfer and Catalyst Layer Thickness on Photocatalytic Reaction", *AIChE J.*, 46(5), p. 1034 (2000).
19. Mehrotra, K.; Yablonsky, G.; Ray, A. K. "Effect of Various Macro-Kinetic Parameters on Photocatalytic Degradation of Benzoic Acid: some further Insights", submitted to *Environmental Science Technology* (2002).

20. Andereck, C. D.; Liu, S. S.; Swinney, H.L. "Flow Regimes in a Circular Couette System with Independently Rotating Cylinders", *Journal of Fluid Mechanics*, pp. 164, 155 (1986).

Author Ajay K. Ray, Ph.D., is an associate professor in the Department of Chemical and Environmental Engineering at the National University of Singapore. Prior to joining the university in 1995, he was with the University of Groningen, The Netherlands for three years. His research interests are in chemical reaction engineering, especially photocatalysis and design, development, simulation, optimization, and analysis of chemical reactors. He holds a Ph.D. in chemical engineering from the University of Minnesota.

This paper was presented at ULTRAPURE WATER Asia 2002, Aug. 14-15, Singapore.

Keywords: MONITORING, WATER QUALITY

TABLE A
Geometric Dimensions and Conditions Used for Different Simulation Runs

Specification	*Case 1 (Reference)*	*Case 2*	*Case 3*
Length L, m	0.425	0.425	0.425
Inner radius r_i, m	0.0434	0.0434	0.0434
Outer radius r_o, m	0.0523	0.0523	0.0523
Annular gap, d, m	0.0089	0.0089	0.0089
Aspect ratio, L/d	47.70	47.70	47.70
Rotation speed, ?, rad/s (rpm)	0.655 (6.25)	0.984 (9.39)	1.638 (15.65)
Volume of liquid treated, V_L m^3	1.136×10-3	1.136×10-3	1.136×10-3
Reynolds Number, Re	253	380	633
Taylor Number, Ta	13,126	29,625	50,116

TABLE B
Comparison of Performance of TVR with that of a Slurry Reactor*

	Slurry Reactor	*Taylor Vortex Reactor*	
	Mehrotra et al., 2002	*Case 1*	*Case 2*
Volume of reactor, m^3	6.35×10-5	3.65×10-3	3.65×10-3
Catalyst surface area, m^2	3.7	0.116	0.116
‡ ICD, ?, m^2/m^3	6,139	102	102
Volume of liquid treated, m^3	2.50×10-4	1.136×10-3	1.136×10-3
Electrical energy input, W	125	30	30
Time for 50% conversion, s	210	128	108
§ Efficiency, s^{-1} m^{-3} W^{-1}	0.0762	0.1146	0.1358
% increase in efficiency	0	50.4	78.3

*For photocatalytic degradation of benzoic acid.
‡: Illuminated catalyst density defined as illuminated catalyst surface area (m^2) per unit volume of liquid treated (m^3) in the reactor (see Reference 10).
§: Efficiency is defined as 50% pollutant (benzoic acid) converted per unit time (s) per unit volume of liquid treated (m^3) per unit electrical energy input (W).